The Institution of Engineering and Technology WILEY

ORIGINAL RESEARCH PAPER

On the modelling, analysis, and design of a suboptimal controller for a class of wind/PV/battery based DC microgrid

Mohammad Reza Arabshahi[1] | **Hossein Torkaman**[1] | **Mehdi Bagheri**[2] | **Ali Keyhani**[3]

[1] Faculty of Electrical Engineering, Shahid Beheshti University, Tehran, Iran

[2] Nazarbayev University, Department of Electrical and Computer Engineering, Nur-Sultan, Kazakhstan

[3] Department of Electrical and Computer Engineering, Ohio State University, Ohio, Ohio, USA

Correspondence

Hossein Torkaman, Faculty of Electrical Engineering, Shahid Beheshti University, Bahar St., Tehran, Iran.
Email: h_torkaman@sbu.ac.ir

Abstract

This study deals with the comprehensive modelling, analysis, and control of a DC microgrid (MG) in islanded mode. The proposed DC MG comprises a wind turbine, a photovoltaic (PV) source, battery storage, DC/DC source, and load side converters with DC loads. To this aim, a circuit-oriented modelling of the whole system is developed. The PV source is modelled with a single-diode electrical circuit. Afterward, a mathematical model of the system with state-space representation was derived. A detailed analysis of PV system design is performed because the parameters of PV are appearing in the dynamic model of DC MG. For the purpose of controller development, the dynamic model of the DC MG, which is modelled by a non-linear-non-affine eight-order system, is linearized around an equilibrium point using the Jacobian matrix framework, while stability using eigenvalue is carried out showing that the stability is guaranteed under operating condition. Finally, for the first time, the state-dependent Riccati equation (SDRE) technique is proposed to find the optimal regulation problem for the DC MG with non-linear-non-affine dynamics. The numerical simulation studies first confirm the validity of the performed mathematical, then the effectiveness of the proposed non-linear controller is evaluated under illumination and load change.

1 | INTRODUCTION

1.1 | Motivation

Nowadays, due to the high price of fossil fuels, the tendency to utilize clean energy resources such as wind and solar energy has significantly increased. It is believed that the fastest photovoltaic technology and reductions in installation costs may be effective solutions for reducing dependency on conventional power systems [1, 2]. Recently, the microgrids (MGs) concept has emerged due to the need for an electric power supply in remote and rural areas, data centres, and electric vehicles (EVs) [3]. MGs are small grids that generally incorporate several distributed generators (DGs) such as photovoltaic (PV) arrays and batteries, loads, and energy storage systems [4, 5]. MGs can operate in parallel with the main grid, and the loads are often fed through the local sources or the main grid [6]. However, in

emergencies such as external disturbances, the corresponding generators and loads in MGs may unplugged from the grid and operate as an islanded MG [7]. Therefore, the ability of MGs to operate in islanded mode can significantly reduce the consumption of electricity and thus, enhance the reliability of the grid. In recent years, DC MGs have become promising structures and attracted more interest than AC MGs due to several inherent characteristics, such as the lack of reactive power, easier control strategy design, and cost-effective low-loss DC/DC converters. The worldwide application of DC MGs in more-electric aircraft, ship MGs, the International Space Station (ISS), and data centres, reveals the employment of DC MGs [10, 11]. A plethora of research on modelling, analysis, design, and control strategies of DC/DC converters, whether loaded by constant power loads (CPLs), resistive loads, and other types of loads, have been reported [12–14]. In DC MGs, the modelling and control problems become more complex as the numbers of DGs and loads

FIGURE 1 One-line diagram of a typical hybrid wind/PV/battery based DC MG
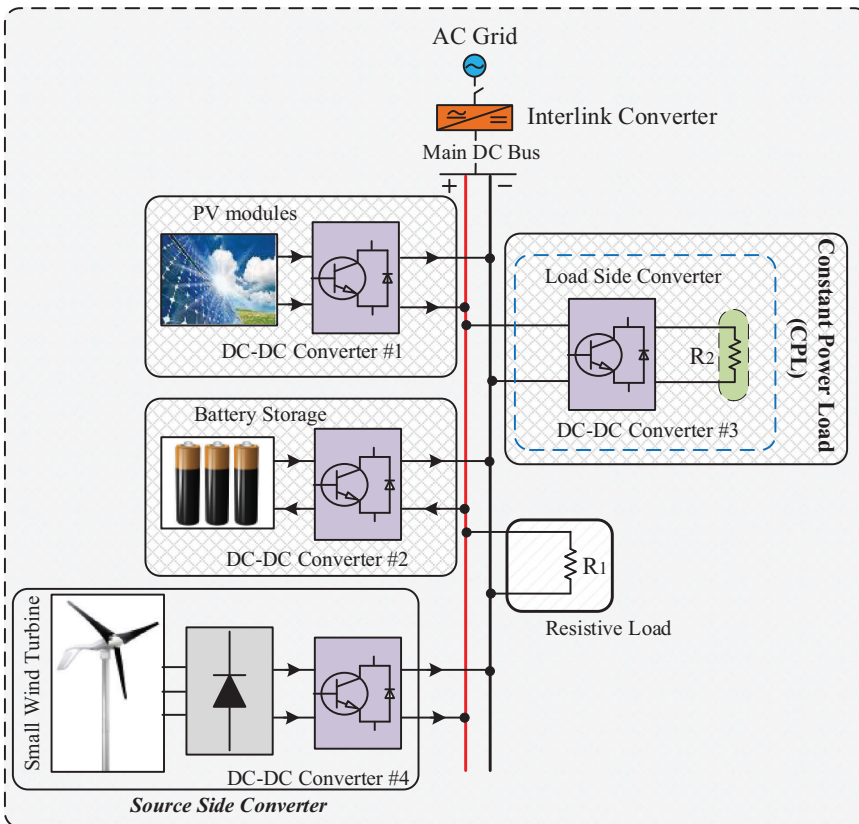
dramatically increased. To this aim, several methods have been proposed by researchers over the years, which will be discussed in the literature.

1.2 | Literature review

In the typical DC MG in the islanded mode as depicted in Figure 1, DC sources are generally connected to DC-link by source-side DC/DC converters. According to Figure 1, when multiple DC/DC converters and loads are connected to a common DC bus, the problem of modelling and analysis becomes challenging. A systematic way to model the DC MG system is to model each component by its electrical circuit.

The PV system, which is connected to the DC bus through a boost converter, is modelled thereby creating an electrical circuit. A good candidate for this modelling is generally called the single-diode model. The majority of research considered this model in their studies as it is simple [8–10]. Usually, the wind turbine and PV modules can operate either in maximum power point tracking (MPPT) or voltage mode control (VMC) which is related to power management strategy, battery state of charge (SOC), and load conditions. Many techniques such as perturbation and observation (P&O) [11], adaptive fuzzy-logic [12], distributed MPPT [13], and genetic algorithm-based optimization MPPT [14] etc., have been used to track MPP at various operating conditions. When the PV source is operated in MPPT, the battery storage could be either in the charge or discharge mode which is dependent on the load levels.

Therefore, the battery is responsible for power balancing among the DGs and loads. A DC/DC converter with bidirectional power flow capability is essential to allow power-sharing between the battery and the other DGs [5]. From the load point of view, a load with DC/DC converters, when tightly regulated can be viewed as a CPL. Also many techniques have addressed the control issue of the bidirectional DC/DC converter loaded by CPL such as sliding mode and passivity-based control [15, 16].

Up to now, many efforts have been dedicated to several aspects of DC MGs such as control, stability analysis, power-sharing method, and modelling. Within this context, the commonly used decentralized droop control method for low-voltage DC MG has been proposed in [17]. A hierarchical three-layer control framework, consisting of primary, secondary, and tertiary control has been presented in [18]. The stability analysis of a DC MG using the Nyquist criterion has been studied in [19], while in [20], a robust stability analysis has been proposed. To facilitate the synthesis of a modular DC nano grid system, a loss-free resistor (LFR) modelling concept has been developed in [21]. In a typical DC MG, switching converters are time-varying non-linear dynamical systems. Moreover, since the PV source has at least one diode in the lumped circuit model, therefore the whole system is highly non-linear. According to Figure 1, there are four basic DC/DC converters in the system. Likewise, many non-linear and linear strategies have been proposed in the literature for the control of DC MGs either without CPLs or at the presence of CPLs. For instance, adaptive back-stepping control [22], sliding-mode

approach [23], passivity-based method [24, 25], linear designs such as the classical LQR problem [26] etc., have also been studied.

In the absence of CPLs, studies have focused on the voltage regulation problem. A robust sliding mode framework was proposed in [23], were applied to DC/DC boost converter to mitigate the instabilities caused by negative incremental impedance of the CPLs. A passivity-based concept was developed in [25], applied to a DC MG with a non-linear-non-affine system model under parametric uncertainty for output voltage regulation. The linear methods are designed based on the linearized models of the system, whose operations are limited around an equilibrium point. Generally, linear control methods adopted the Jacobian linearization framework to linearize system. For example, the quadratic regulation for linear systems, called LQR, was successfully applied in a wide variety of applications, such as switching power converters [26], an inverted pendulum [27], and unmanned quad-rotor helicopter [28], however, many studies were focused on control systems with non-linear dynamics.

Recently, studies [29, 30] addressed the State-Dependent Riccati Equation (SDRE) strategy as a striking tool for the systematic design of non-linear feedback controllers for a broad class of non-linear, affine, and non-affine systems. The main idea behind this theory is to bring the non-linear system to a state-dependent linear system using a process called extended linearization.

Most of the earlier research in the control and stability analysis of DC MG considers single or two DC/DC converters in their analysis and ignores the rest of the DC MG. Moreover, the PV source is generally modelled by a constant voltage source [31]. On the contrary, in this paper, the PV source is modelled by a well-known and practical model [8, 10]. As will be shown later, the dynamic model of the proposed DC MG in this study is a system with a non-linear-non-affine structure. This matter motivated us to develop the SDRE based non-linear feedback control technique for a class of wind/PV/battery based DC MG with non-linear-non-affine dynamics as it is suitable for regulation the states variables to converge to their equilibrium points.

1.3 | Main contributions

In spite of the fact that the whole DC MG system is an integration of conventional DC/DC power converters and well-known models of PV as well as a battery; however, this paper deals with a more complex network topology when compared to previous research works in [24, 25]. On the other hand, this paper deals with a more realistic system. Then, mathematical details corresponding to our developed model are presented.

The proposed DC MG has a typical structure and consists of a small wind turbine, a PV system, battery storage, DC/DC converters, a resistive load, and a CPL. We utilized a circuit-oriented modelling approach to address the modelling of the DC MG. In this regard, at the first step, we used the single-diode model of the PV source. It will be shown in Section 3

that the parameters related to the PV source can be observed in the state-space model. There are five parameters, usually called unknown parameters [32], in the module and corresponding values in a PV plant those are the photo-generated current (I_{ph}), dark saturation current (I_o), diode ideality factor (D), series (R_s), and shunt (R_{sh}) resistances. We use a system of implicit/explicit equations to find the values of those parameters. Some of these parameters are needed to be estimated. Therefore, this paper proposed to find the value of those parameters using simple classical Gauss-Seidel (GS) algorithms. Notably, it is not mandatory to use the GS method, however, the convergence is satisfactory [32]. It is also shown that by applied mathematics, the PV source can operate under various irradiance. Afterward, we established our hybrid DC MG using the state-space model. In summary, the main contributions of this paper are as follows:

- A detailed modelling and analytical analysis are developed for DC MG comprising wind/PV/battery sources in this paper. This kind of systematic modelling gives more insight into the system design and operation.
- The DC MG dynamical model is expressed by $\dot{x}(t) = f(x(t), u(t))$. Detailed analysis of the Jacobian linearization process for an eight-order DC MG system around an operating point is conducted; then, the model is represented in the form of the state-space model. In addition, the determination of the eight-order state-space time domain is a non-trivial task since the system is highly non-linear and non-affine, respectively. Moreover, the eigenvalue diagram of the system is plotted to demonstrate the stability of the system. The numerical simulation results which are generated in MATLAB confirm the correctness of the linearization process.

Up to now, the analysis and output voltage regulation of DC MG with non-linear-non-affine structure have been performed and elaborated in [24] and [25], while, in this study, for the first time, the application of a non-linear control method based on SDRE regulator for a DC MG system comprising hybrid wind/PV/battery model is examined. Furthermore, the PV modelling part has more elaborated with valid and reasonable techniques. The SDRE regulator is successfully applied to the system. The conducted analysis shows the superiority of the non-linear feedback controller over the linear one and constant linear feedback when both illumination and load change occur.

1.4 | Paper organization

The rest of this paper is organized as follows: Section 2 addresses detailed system modelling, including load, converters, wind turbine, and PV generator models. Section 3 is dedicated to a linear and non-linear representation of the DC MG system. The design of the linear quadratic regulator framework is presented in Section 4. The concept of the proposed non-linear controller is studied in Section 5. Section 6 uses the simulation tests to verify the theory by performance evaluation. Eventually, conclusions are drawn in Section 7.
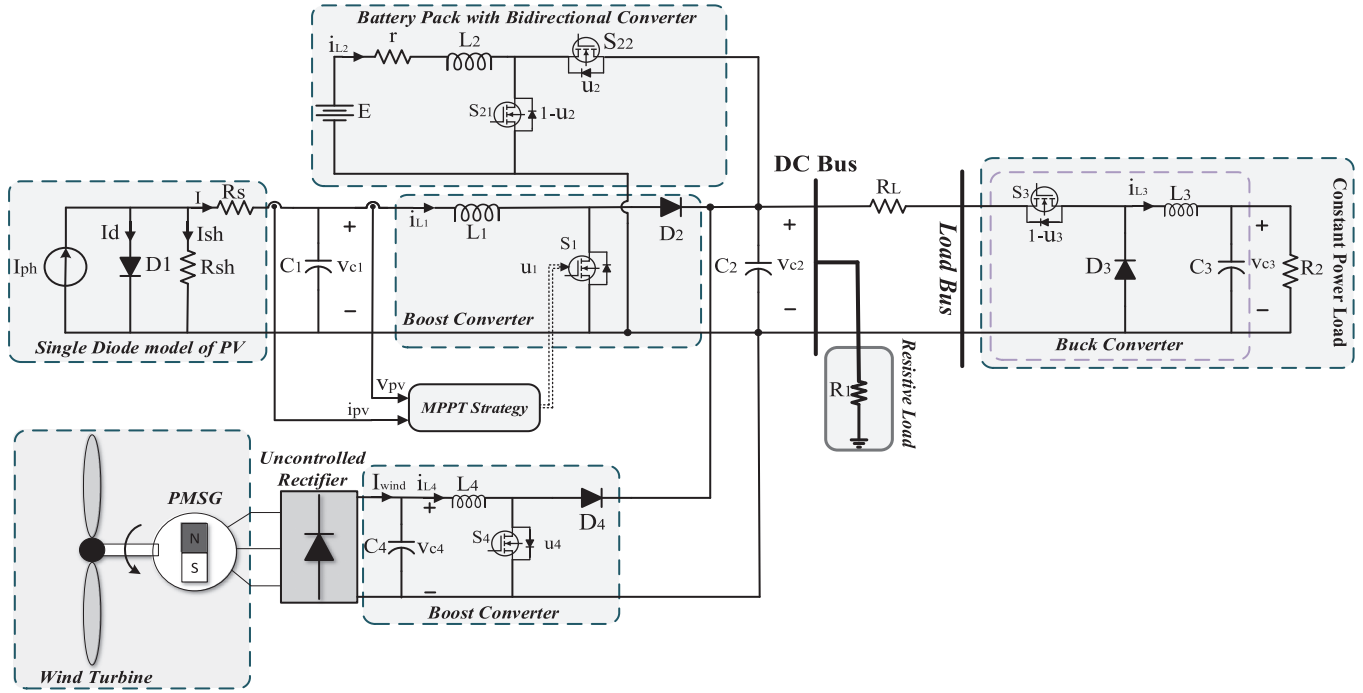
FIGURE 2 Proposed DC MG equivalent electrical circuit

2 | MATHEMATICAL MODELLING OF THE PROPOSED DC MG IN ISLANDED MODE

To start our analysis, each component in the DC MG should be modelled. This kind of modelling gives us insight from inside the system. Accordingly, the electrical model of the battery and loads are specified first, then PV source and wind turbine are modelled as well.

2.1 | Battery, load, and converters model

An electrical circuit of the DC MG in islanded mode is shown in Figure 2. The DC MG consists of a PV system, which is connected to a DC bus through a DC/DC boost converter. Likewise, a wind turbine energy conversion system is connected to the DC bus using a DC/DC boost converter. A bidirectional DC/DC converter is used for the integration of the battery storage system. The battery storage is modelled via electromotive force (E) with an internal resistor(r). One of the loads is (R_1) directly connected to the main DC bus, and the other load is a combination of the DC/DC buck converter and resistance (R_2). Since the output voltage of the buck converter is tightly regulated, the converter with load together consumes constant power [24]. Moreover, a line resistor R_L represents the loss of the transmission line and u_i ($i = 1, 2, 3, 4$) is the duty cycle of the switches. It is assumed that the PV source with a single-diode model feeds the DC MG.
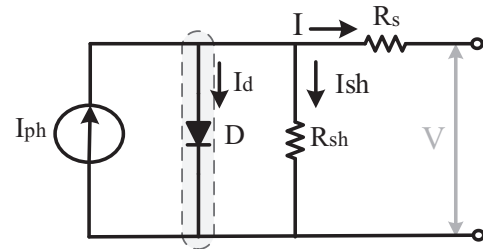

FIGURE 3 Single-diode electrical equivalent circuit of the PV generator [10]

2.2 | Modelling of the PV source in the DC MG

There are many options to model a PV, including the single-diode, double-diode, and even triple-diode models [10]. In this study, the PV generator is modelled via a current source in parallel with a diode and a shunt resistance. Moreover, a resistor is connected in series as shown in Figure 3. With the application of Kirchhoff's current law, the relationship between the terminal voltage (V) and current (I) of PV can be described by the following equation [10]:

$$I = I_{ph} - I_d - I_{sh} \tag{1}$$

$$I = I_{ph} - I_o \left\{ \exp\left(\frac{V + R_s I}{n V_t} \right) - 1 \right\} - \frac{V + R_s I}{R_{sh}} \tag{2}$$

where n is the number of cells in the PV module connected in series, and V_t is the thermal voltage junction of the PV.
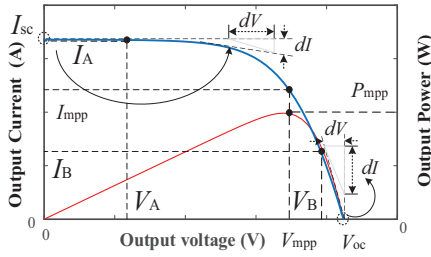
FIGURE 4 Three major key points on output characteristics of PV source [10]

The thermal voltage is mainly stated as [10]:

$$V_t = \frac{KTD}{q} \tag{3}$$

where K is Boltzmann's constant (= 1.389×10^{-23} J/(°K)), q is defined as the electron charge (= 1.609×10^{-19} (°C)), D is the diode ideality factor, and T is the temperature. In the manufacturer's datasheet, the following information always exists for the standard test conditions (STC: temperature, 25 °C; irradiance, 1000 W/m^2): short−circuit current I_{sc}; open-circuit voltage V_{oc}; voltage V_{mpp} and current I_{mpp} at the maximum power point (MPP); temperature coefficient for the short-circuit current; and open-circuit voltage (K_i, K_v). There are three major key points on every $I - V$ characteristic. These major key points, $(0, I_{sc})$, $(V_{oc}, 0)$, and (V_{mpp}, I_{mpp}), are illustrated in Figure 4 [10, 32].

Usually, it is suggested to use the information available in the module datasheet to extract the unknown parameters. These unknown parameters were discussed previously. With the substitution of these major key points into Equation (2), a set of equations are derived at STC as follows [10]:

$$V_t = \frac{R_s I_{mpp} + V_{mpp} - V_{oc}}{n \ln \left\{ \frac{(I_{sc} - I_{mpp})(R_s + R_{sh}) - V_{mpp}}{I_{mpp}(R_s + R_{sh}) - V_{oc}} \right\}} \tag{4}$$

$$R_s = \frac{V_{oc} - V_{mpp} + nV_t \ln(\lambda)}{I_{mpp}} \tag{5}$$

where λ in (5) is calculated by

$$\lambda^{-1} = \frac{V_{mpp} I_{sc}(R_s + R_{sh}) + I_{sc} R_s I_{mpp}(R_s + R_{sh})}{nV_t(I_{mpp} R_{sh} + I_{mpp} R_s - V_{mpp})}$$
$$+ \frac{V_{oc}(I_{mpp} R_s - V_{mpp})}{nV_t(I_{mpp} R_{sh} + I_{mpp} R_s - V_{mpp})}.$$

The R_{sh} value at STC can be derived as:

$$R_{sh} = \frac{nV_t(R_s + R_{sh}) + R_s \exp(\beta)(I_{sc} R_s + I_{sc} R_{sh} - V_{oc})}{nV_t + \exp(\beta)(I_{sc} R_s + I_{sc} R_{sh} - V_{oc})} \tag{6}$$

where β is calculated by $\beta = (I_{mpp} R_{sh} - V_{oc} + V_{mpp})/nV_t$.

TABLE 1 The extracted parameters for the single module and 1 kW array at STC

Datasheet parameters [34]	Estimated for module	Equivalent array
$I_{sc} = 8.13$ A	$I_{ph} = 8.13$ A	$I_{ph} = 16.26$ A
$V_{oc} = 30.6$ V	$I_o = 0.038\ \mu$A	$I_o = 0.076\ \mu$A
$I_{mpp} = 7.58$ A	$D = 1.242$	$D = 1.242$
$V_{mpp} = 24.4$ V	$R_{s0} = 0.4\ \Omega$	$R_s = 0.368\ \Omega$
K_i(mA/°C)=4.39	$R_{sh0} = 1500\ \Omega$	$R_{sh} = 2563\ \Omega$
K_v(mV/°C)=−104.95	$R_s = 0.245\ \Omega$	$I_{mpp} = 15.16$ A
$n = 50$	$R_{sh} = 1708.7\ \Omega$	$V_{mpp} = 73.2$ V

It is observed from (5) and (6) that these two equations are implicit in nature. Therefore, an iterative-based method like the GS may be used to extract three unknown parameters [32]. Further information associated with the GS method is addressed in [32], while the flowchart of the whole algorithm is shown in Figure 5. The error criteria are defined as Error(%) = $|(x_{i+1} - x_i)/x_{i+1}| \times 100$, and ε is the predefined mismatch (1e $^{-6}$). It is noteworthy that the values of R_s and R_{sh} in (5) and (6) should be initialized to start the GS algorithm because the equations are transcendental [32].

The selection of a suitable initial value is a critical step in starting iterative algorithms. Generally, the value of R_s is low (0 ∼ mΩ), whereas R_{sh} is high (in the range of kΩ) [10]. According to Figure 4, these two parameters are initialized at:

$$R_{si} = (V_{oc} - V_B)/I_B \tag{7}$$

$$R_{shi} = V_A/(I_{sc} - I_A) \tag{8}$$

where R_{si} and R_{shi} are the initial values for R_s and R_{sh}, respectively, $V_A \cong 0.2V_{oc}$ and $I_B \cong 0.2I_{sc}$ [33]. After numerically extracting V_t, R_s and R_{sh}, the remaining parameters can be analytically derived. These two parameters, I_o and I_{ph}, are given as:

$$I_o = \left(I_{sc} - \frac{V_{oc} - I_{sc} R_s}{R_{sh}} \right) \exp \left(-\frac{V_{oc}}{nV_t} \right) \tag{9}$$

$$I_{ph} = I_o \exp \left(\frac{V_{oc}}{nV_t} \right) + \frac{V_{oc}}{R_{sh}} \tag{10}$$

Now, all equations needed to extract the five unknown parameters have been obtained. A UD−185MF5 Mitsubishi module datasheet [34] is selected as the case study module, and the unknown parameters are extracted via the proposed procedure. After extracting five unknown parameters under the STC, all these parameters can be substituted in the $I–V$ characteristic Equation (2) for $0 \leq V \leq V_{oc}$ to obtain the current. Since $I–V$ characteristic equation is an implicit equation, the iterative technique must be applied [10]. The same procedure as mentioned in the earlier study [32] is used in this paper to construct a PV power plant. The extracted parameters for the module and corresponding parameters for the 1-kW array are given in Table 1.
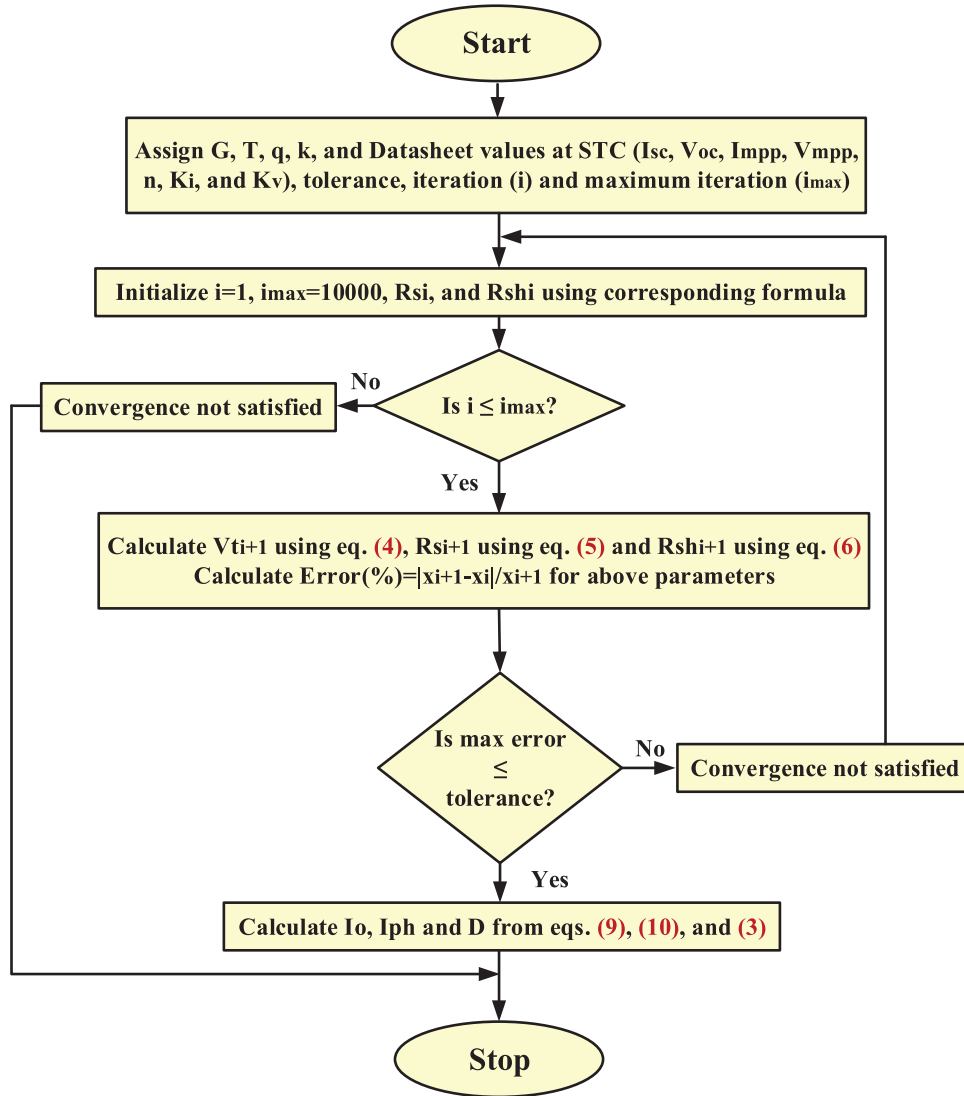
FIGURE 5 The flowchart of the GS algorithm for extracting unknown parameters of PV [32]

It is seen from Table 1 that the value of I_{ph} is equal to I_{sc}. This is not unexpected, however, these two parameters are nearly identical [35]. The I–V and P–V characteristic curves for the module as well as the 1-kW array are depicted in Figure 6.

Notably, the PV source model characteristic which is taken from simulink environment is plotted in Figure 6c,d next to the model used in this paper. As can be seen, both $I - V$ and $P - V$ characteristic are nearly identical at STC.

Furthermore, the convergence paths of the GS method for R_s and R_{sh} are also plotted in Figure 6d. It is assumed that " $= 10^{-6}$. Accordingly, after a number of iterations, the convergence criterion is satisfied. As will be shown in the following section, the PV source parameters like R_s, R_{sh} etc., would appear in the dynamic state-space model of DC MG. The previous analysis provides a better understanding of the PV system design and operation which is ignored in the same earlier research works [24, 25].

2.3 | Modelling of wind turbine

A typical structure of a wind turbine energy conversion system was shown in Figure 2. The model involves a wind turbine, a permanent magnet synchronous generator, and a rectifier. The rectifier is used to convert AC power to DC, whilst the boost converter is responsible for adjusting the wind turbine power by means of switching function regulation.

Usually, the mechanical power which is captured by a wind turbine can be calculated by [36]:

$$P_{mech} = \frac{1}{2}\rho A_r C_p \left(\lambda, \beta_{wind} \right) v_w^3 \qquad (11)$$

where ρ is the air density; A_r is the area swept by the wind blades; v_w is the wind speed; and C_p is the power coefficient. The power coefficient, C_p, is obtained by the blade pitch angle
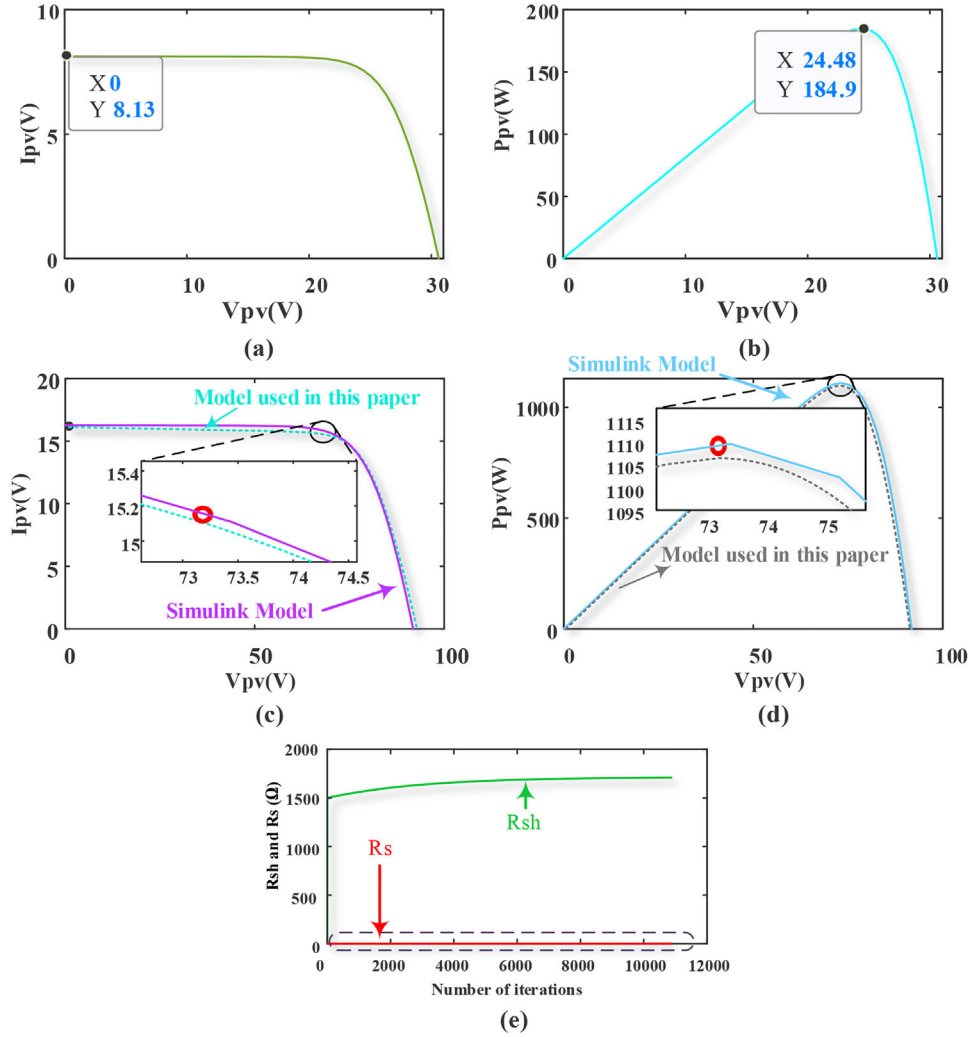
FIGURE 6 Output characteristics under STC: (a) I − V for a module, (b) P − V for a module, (c) I − V for the 1-kW array, (d) P − V for the 1-kW array, (e) The convergence paths of R_s and R_{sh} obtained by the GS method

(β_{wind}) which is constant during MPPT control and tip speed ratio as given by [36]:

$$\lambda = \frac{\omega_t R_b}{v_w} \qquad (12)$$

where R_b is the blades radius and ω_t is the rotating speed. For a typical wind turbine, $C_p - \lambda$ plot is given in Figure 7a.

As shown in Figure 7a, there is an optimal point on the $C_p - \lambda$ curve, which is implied that the power coefficient may reach its maximum value C_{pmax} if the rotor speed can be adjusted so that the turbine operates at optimum tip speed ratio λ_{opt}. Figure 7b, shows the power rotor speed characteristic curves for different wind speeds where the optimum power line represents the maximum power points. For the PMSG, the electromotive force E_g is proportional to the generator speed, which is determined by [36]:

$$E_g = \frac{4.44}{4\pi}\psi_{PM}N_P\omega_m \qquad (13)$$

where ψ_{PM} is the flux linkage of the PMSG, N_P is the number of pole pairs, and ω_m is the shaft speed of the generator. Accordingly, if the aerodynamic power is captured from the wind turbine and fed PMSG, the phase terminal voltage V_t would be [36]:

$$V_t = E_g - I_a (R_s + j\omega_m L_S) \qquad (14)$$

where I_a is the phase current, R_s is the stator phase resistance, and L_S is the stator phase inductance. The generator rectifier voltage can be then realized as [36]:

$$V_{link} = \frac{3\sqrt{6}}{\pi} V_t \qquad (15)$$

where V_{link} denotes the DC-link voltage or input voltage of the boost converter. The following section aims to study the nonlinear and linearized dynamic models of the DC MG.
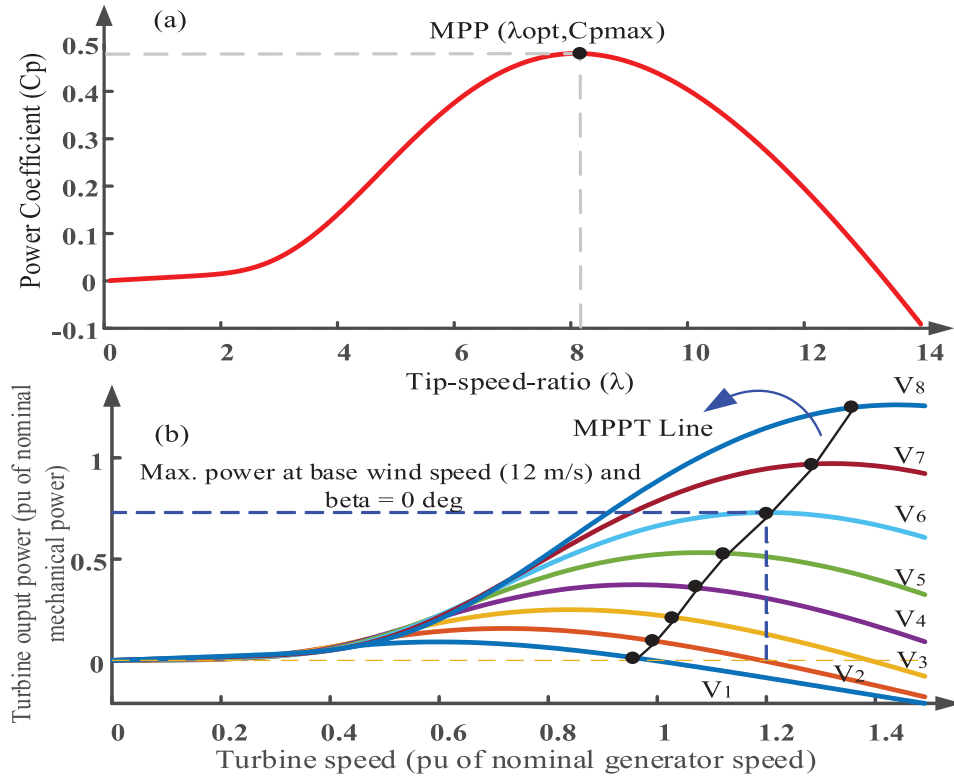
FIGURE 7 Typical characteristics of wind turbine: (a) $C_p - \lambda$ curve (b) power-rotor speed characteristic curves for different wind speeds

3 | NON-LINEAR AND LINEARIZED MODELS OF DC MG FOR CONTROLLER DEVELOPMENT

This section addresses the complete modelling of the DC MG shown in Figure 2 in the state-space non-linear and linear forms. Accordingly, with the application of Kirchhoff's current (KCL) and voltage (KVL) laws in the DC/DC boost converter, one can obtain the following equations:

$$L_1 \frac{di_{L_1}}{dt} = v_{C_1} - v_{C_2} (1 - u_1) \tag{16}$$

$$C_1 \frac{dv_{C_1}}{dt} = I_{ph} - I_o \left(\exp \left(\left(v_{C_1} + i_{L_1} R_s \right) a \right) - 1 \right) - \frac{v_{C_1} + i_{L_1} R_s}{R_{sh}} - i_{L_1} \tag{17}$$

where a in (17) is equal to $a = 1/(nV_t)$. For the DC/DC bidirectional buck-boost converter, it can be written as:

$$L_2 \frac{di_{L_2}}{dt} = E - ri_{L_2} - v_{C_2} u_2 \tag{18}$$

$$C_2 \frac{dv_{C_2}}{dt} = i_{L_1} (1 - u_1) + i_{L_2} u_2 - \frac{v_{C_2}}{R_1} - i_{L_3} (1 - u_3) + i_{L_4} (1 - u_4) \tag{19}$$

Similarly, considering KCL and KVL in the DC/DC buck converter, one can obtain:

$$L_3 \frac{di_{L_3}}{dt} = \left(v_{C_2} - i_{L_3} R_L (1 - u_3) \right) (1 - u_3) - v_{C_3} \tag{20}$$

$$C_3 \frac{dv_{C_3}}{dt} = i_{L_3} - \frac{v_{C_3}}{R_2} \tag{21}$$

Finally, based on KVL, and KCL, the following set of differential equations are obtained:

$$L_4 \frac{di_{L_4}}{dt} = v_{C_4} - (1 - u_4) v_{C_2} \tag{22}$$

$$C_4 \frac{dv_{C_4}}{dt} = I_{wind} - i_{L_4} \tag{23}$$

The corresponding constraints are defined as follows: $v_{C_2} > 0$, $v_{C_3} > 0$, $i_{L_1} \geq 0$, $i_{L_3} \geq 0$, $i_4 \geq 0$

In the Equations (16)–(23), i_{L_i} and v_{C_i} ($i = 1, 2, 3, 4$) are the instantaneous inductor current and capacitor voltage, respectively, u_1 are the switching function of the converters or control input signals and I_{wind} is the injected current to the DC MG by the wind turbine, respectively. In the next subsection, the non-linear system will be linearized around an equilibrium point.

3.1 | Non-linear model and linearization around an equilibrium point

Let us reform and model the system into the general state-space form as $\dot{x}(t) = f(x(t), u(t))$. Obviously, voltage and current of the capacitors and inductors are the state variables which are represented by: $x^T = [x_1 \ x_2 \ x_3 \ x_4 \ x_5 \ x_6 \ x_7 \ x_8] = [i_{L_1} \ v_{C_1} \ i_{L2} \ v_{C_2} \ i_{L_3} \ v_{C_3} \ i_{L_4} \ v_{C_4}]$

Therefore, the averaging state-space model of the system can be rewritten as:

$$f(x, u) = \begin{cases} \frac{1}{L_1}(x_2 - x_4(1 - u_1)) \\ \frac{1}{C_1}\left(I_{ph} - I_o\left(e^{a(x_2 + R_s x_1)} - 1\right) - \frac{x_2 + R_s x_1}{R_{sh}} - x_1\right) \\ \frac{1}{L_2}(E - rx_3 - x_4 u_2) \\ \frac{1}{C_2}\left(x_1(1 - u_1) + x_3 u_2 - \frac{x_4}{R_1} - x_5(1 - u_3) + x_7(1 - u_4)\right) \\ \frac{1}{L_3}\left(x_4(1 - u_3) - x_5 R_L(1 - u_3)^2 - x_6\right) \\ \frac{1}{C_3}\left(x_5 - \frac{x_6}{R_2}\right) \\ \frac{1}{L_4}(x_8 - x_4(1 - u_4)) \\ \frac{1}{C_4}(I_{wind} - x_7) \end{cases}$$

(24)

With these constraints: $x_2 > 0, x_6 > 0, x_1 \geq 0, x_5 > 0$ and $x_7 > 0$. It is observed from (24) that we have to deal with an eighth-order non-linear-non-affine system. It should be noted that for the sake of simplicity, all time-domain variables (e.g. $x(t)$ and $u(t)$) are shown as x and u. Because the state variables are multiplied by the control signals, the system becomes non-linear, and due to the existence of non-linear control input u_3^2, the system becomes non-affine. In the following, we consider the stability of the dynamic model of the DC MG given in (24). The DC MG system is stable at a given equilibrium point if the state trajectory converges to an equilibrium point with a small disturbance. This means that the system is stable if all of the eigenvalues of the linearized system around an equilibrium point have a negative real part.

Supposing that $u^T = [u_1 \ u_2 \ u_3 \ u_4] = [0 \ 0 \ 0 \ 0]$, then $\dot{x} = 0$ is solved to find the equilibrium points of the unforced system:

$$\overset{*}{x}_2 - \overset{*}{x}_4 = 0 \rightarrow \overset{*}{x}_2 = \overset{*}{x}_4 \tag{25}$$

$$I_{ph} - I_o\left(e^{a\left(\overset{*}{x}_2 + R_s \overset{*}{x}_1\right)} - 1\right) - \frac{\overset{*}{x}_2 + R_s \overset{*}{x}_1}{R_{sh}} - \overset{*}{x}_1 = 0 \tag{26}$$

$$E - r\overset{*}{x}_3 = 0 \rightarrow \overset{*}{x}_3 = \frac{E}{r} \tag{27}$$

$$\overset{*}{x}_1 - \frac{\overset{*}{x}_4}{R_1} - \overset{*}{x}_5 + \overset{*}{x}_7 = 0 \tag{28}$$

$$\overset{*}{x}_4 - \overset{*}{x}_5 R_L - \overset{*}{x}_6 = 0 \tag{29}$$

$$\overset{*}{x}_5 - \frac{\overset{*}{x}_6}{R_2} = 0 \rightarrow \overset{*}{x}_5 = \frac{\overset{*}{x}_6}{R_2} \tag{30}$$

$$\overset{*}{x}_8 - \overset{*}{x}_4 = 0 \rightarrow \overset{*}{x}_8 = \overset{*}{x}_4 \tag{31}$$

$$I_{wind} - \overset{*}{x}_7 = 0 \rightarrow \overset{*}{x}_7 = I_{wind} \tag{32}$$

By substituting $\overset{*}{x}_5$ from (30) into (29) and (28), then I_{wind} from (32) into (28), yield: $\overset{*}{x}_1 = -I_{wind} + \left(\frac{R_1 + R_2 + R_L}{R_1 R_2}\right)\overset{*}{x}_6$ and $\overset{*}{x}_2 = \overset{*}{x}_4 = \overset{*}{x}_8 = (1 + R_L/R_2)\overset{*}{x}_6$. Finally, by substitution of $\overset{*}{x}_1$ and $\overset{*}{x}_2$ from the aforesaid equations and $\overset{*}{x}_5$ from (28) into (24), the following equations are obtained as:

$$I_{ph} - I_o\left\{e^{a\left(-I_{wind} + \left(\frac{R_1 + R_2 + R_L}{R_1 R_2}\right)\overset{*}{x}_6\right)} - 1\right\}$$

$$- \frac{1}{R_{sh}}\left(\left(1 + \frac{R_L}{R_2}\right)\overset{*}{x}_6 - I_{wind} + \left(\frac{R_1 + R_2 + R_L}{R_1 R_2}\right)\overset{*}{x}_6\right)$$

$$- \left(\frac{R_1 + R_2 + R_L}{R_1 R_2}\right)\overset{*}{x}_6 = 0 \tag{33}$$

One of the objectives of control in this study is that the PV output power (P_{pv}) should always track the maximum value.

Considering Equation (2) corresponds to PV current, a more realistic form of the output power of PV source is calculated by: [10, 32],

$$P_{pv} = I \times V = \left(I_{ph} - I_o\left\{\exp\left(\frac{V + R_s I}{nV_t}\right) - 1\right\} - \frac{V + R_s I}{R_{sh}}\right)V \tag{34}$$

To find the maximum value of P_{pv} using (34), both I and V should be maximized simultaneously. It is seen that solving (34) to find the maximum value of P_{pv} is not a trivial task, as it is a non-linear transcendental equation, however one can take the following reasonable assumptions:

- As mentioned earlier, the value of R_s is nearly zero [32], therefore the approximation of: $\exp(\frac{V}{nV_t}) \gg \exp(\frac{R_s I}{nV_t})$ is valid [35].
- Moreover, the value of R_{sh} is high, in the range of $k\Omega$, considering $R_{sh} \gg R_s$, which means the term of $(R_s I)/R_{sh}$ is negligible as well [35].

Therefore, the output power of the PV source would be rewritten:

$$P_{pv} = I \times V = \left(I_{ph} - I_o\left\{\exp\left(\frac{V}{nV_t}\right) - 1\right\} - \frac{V}{R_{sh}}\right)V \tag{35}$$

The power of PV would be determined using (35), as it only depends on V. At the maximum power point, the derivative of
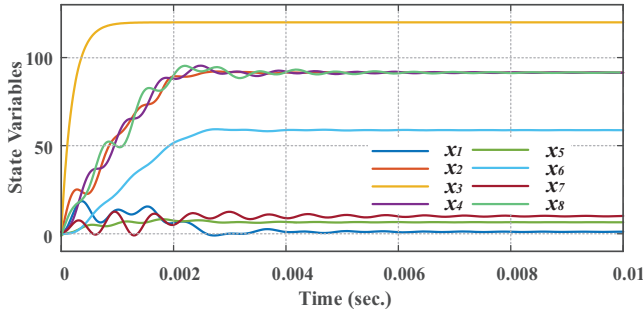
FIGURE 8 A Plot of state variables converge to an equilibrium points

TABLE 2 The given parameters for buck converter

Parameters	Value
Inductor (L_3)	200 μH
Capacitor (C_3)	100 μF
Resistance (R_2)	9 Ω
Critical resistance (R_{crit})	15 Ω
Transmission line (R_L)	5 Ω
Input voltage (V_{in})	270 V
Output voltage (V_{out})	100
Switching frequency (f_s)	20 kHz

P with respect to V is zero [10, 32], therefore one can obtain,

$$I_{ph} - I_o - \frac{I_o V}{nV_t} \exp\left(\frac{V}{nV_t}\right) - \frac{2}{R_{sh}}V - I_o \exp\left(\frac{V}{nV_t}\right) = 0 \tag{36}$$

Now, the maximum value for V in (36), can be determined using numerical solvers which give us the maximum power of the PV source as well, however, other techniques like P&O may be used to find the maximum value of P_{pv}. Meanwhile, the PV source model in our DC MG can operate at various irradiance by only changing the value of I_{ph}.

3.2 | Model verification and eigenvalue analysis

To investigate the stability of the linearized system, the eigenvalues of the Jacobian matrix should be analysed. Solving (33), which is non-linear in nature, yields the solution for $\overset{*}{x}_6$. Subsequently, equilibrium points of the DC MG system can be obtained via finding the solution of $\overset{*}{x}_6$. By linearizing the state-space form according to (24) around an equilibrium point, matrices A and B of the model will be computed as given in Appendix A. The following equilibrium points are obtained as: $\overset{*}{x} = [1.1 \ 91.47 \ 120 \ 91.47 \ 6.53 \ 58.8 \ 10 \ 91.47]^T$

A plot of the state variables without any control inputs $u^T = [u_1 \ u_2 \ u_3 \ u_4] = [0 \ 0 \ 0 \ 0]$ is depicted in Figure 8 with the following initial conditions: $[x_{01} \ x_{02} \ x_{03} \ x_{04} \ x_{05} \ x_{06} \ x_{07} \ x_{08}]^T = [1 \ -1 \ 0.2 \ 1 \ -1 \ 0.2 \ 1 \ -1]$ which shows that the state trajectories gradually converge to their equilibrium points. Besides, two different simulations are carried out for the purpose of validation and demonstrating the accuracy of the state-space model as well. First, a real simulation is accomplished by considering electrical components of DC MG like DC/DC converters, power MOSFETs etc. Moreover, another simulation is done by using the state-space non-linear model. For the sake of simplicity, both simulations is done for the case of the buck converter. The load voltage and current waveforms are depicted in Figures 9a,b which denote the buck converter operates in continuous current mode (CCM). The corresponding parameters for simulation are given in Table 2. Recall that

CCM refers to the current in the inductor remaining positive for the entire switching period. Subsequently, the conversion ratio would be $V_{out} = V_{in}d$ for buck converter means that the output voltage is controlled by adjusting the duty ratio d. However, a different analysis is required for the discontinuous current mode (DCM). In other words, the dynamics will be altered and output voltage does not follow the expression as in CCM which is depicted in Figures 9c and 9d respectively. As can be seen, the difference between the two waveforms is evident. Increasing R_2 more than its critical value (or light load current) leads to DCM. In summary, it can be concluded that for DCM case, the presented dynamics in (20) and (21) are not quite accurate when compared to the real simulation. Further details about mode boundaries for the conventional buck, boost, and buck-boost converter are given in [37].

Through linear state-space representation, eigenvalue-based analysis can be utilized to study the stability of the system. In Figure 10, an eigenvalue diagram of the linearized system is presented. It can be seen from this figure, all eigenvalues have a negative real part, are located in the left half- plane (LHP) of an imaginary axis.

It means that the linearized system around the equilibrium point is stable. Notably, without any control inputs, the state variables converge to their equilibrium point. Therefore, results prove that the linearization process in Appendix A is valid.

3.3 | Objectives of the control

In this paper, four control objectives can be defined for the DC MG which are: $x_2 \to \overset{*}{x}_2 \ x_4 \to \overset{*}{x}_4 \ x_6 \to \overset{*}{x}_6 \ x_8 \to \overset{*}{x}_8$

The objectives $x_2 \to \overset{*}{x}_2$ and $x_8 \to \overset{*}{x}_8$ denote that the setpoints $\overset{*}{x}_2$ and $\overset{*}{x}_8$ should always track maximum power points. For instance, the maximum power point of PV is calculated by (43) using any numerical solvers for a given set of parameters related to PV (i.e. I_{ph}, a, R_{sh}, and I_o). Likewise, in the wind turbine, the maximum power captured from wind is intended. Two remaining objectives belong to DC bus and load voltages which are constant predefined setpoints. To achieve voltage regulation for the hybrid DC MG with the non-affine-non-linear dynamical
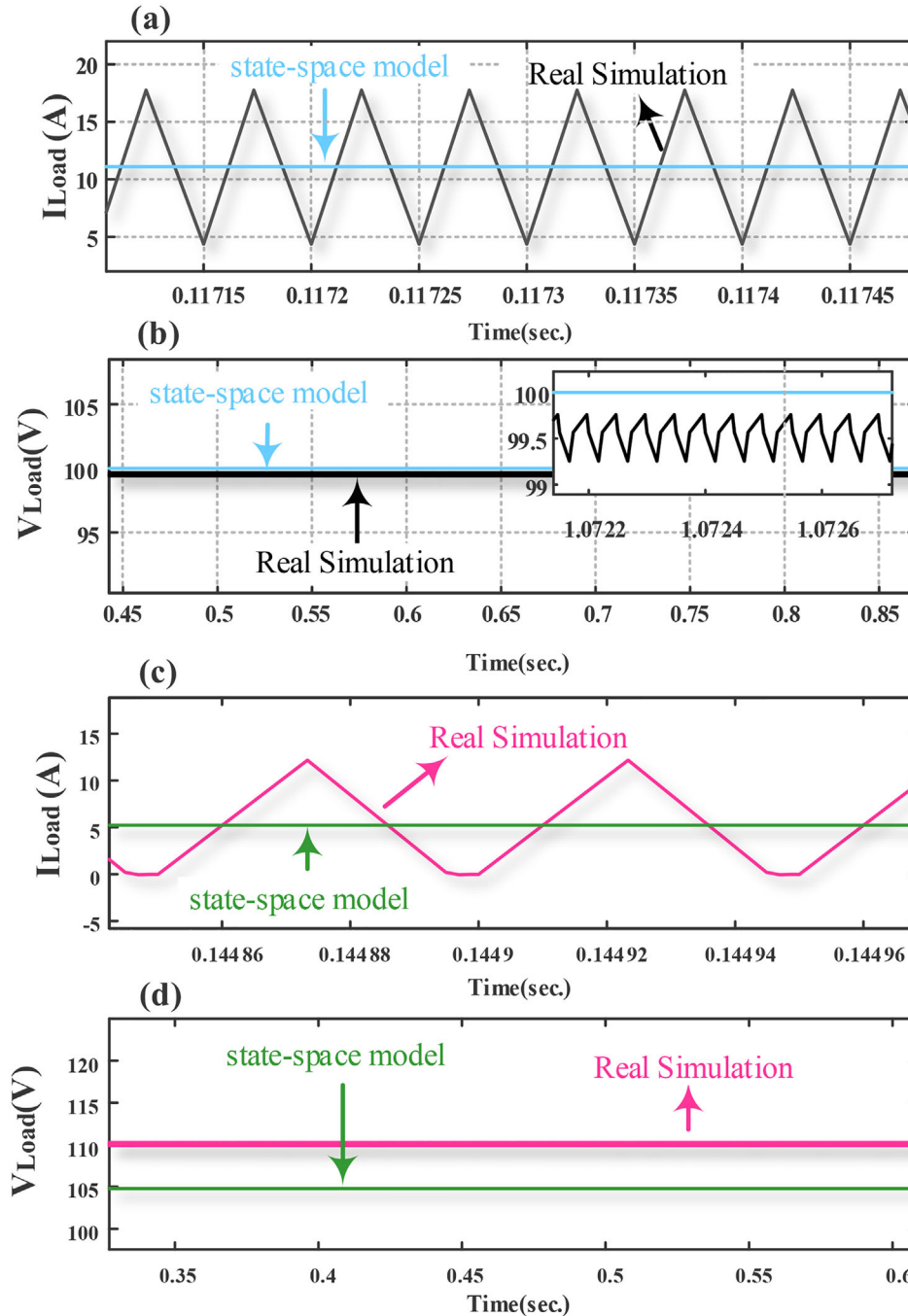
FIGURE 9 Buck converter waveforms in (a,b) CCM and (c,d) DCM

model, we will use a suboptimal non-linear regulator. Now, the linear and non-linear models of the DC MG are obtained. In the next section, we will investigate how to design a control strategy.

4 │ LINEAR QUADRATIC REGULATOR (LQR) CONTROLLER DESIGN

In this section, an LQR regulator controller is developed. The LQR controller offers design flexibility through weighting matrices, and the closed-loop system achieves optimal performance because it is defined by a quadratic cost function. On the other hand, unlike the state feedback controller, the LQR controller locates the eigenvalues where the system has the best dynamic response. The design objective of this controller is to define the feedback law (u) so that the state variables track the desired trajectories and the following cost function is minimized:

$$J = \frac{1}{2} \int_0^\infty \left(x^T Q x + u^T R u \right) dt \qquad (37)$$

FIGURE 10 Eigenvalue diagram of the linearized system
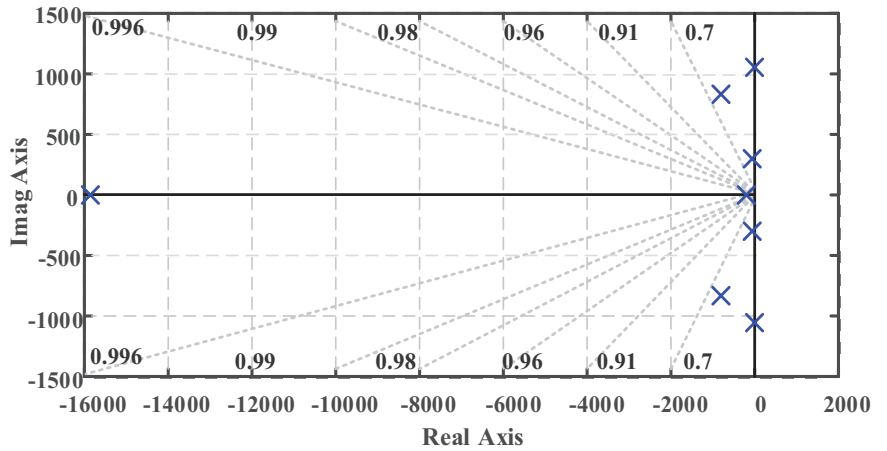
where R and Q are the weighting matrices. The feedback control law is defined as follows:

$$u = -Kx \tag{38}$$

where $K = R^{-1}B^T P$ and P is the solution of Algebraic Riccati Equation (ARE) defined by:

$$A^T P + PA - PBR^{-1}B^T P + Q = 0 \tag{39}$$

The design parameters Q and R are selected so that Q is a positive semidefinite matrix and R is a positive definite matrix. The selection of Q and R is crucial to the stabilization and performance of the system. It is noteworthy that these matrices are taken as diagonal matrices either with only constant values or state-dependent [30, 38]. Moreover, the pair (A, B) is pointwise stabilizable (controllable).

This controllability means that the matrix $Rank([BAB \dots \quad A^{n-1}B]) = \Psi$ should be a full-row rank matrix, where Ψ is the number of state variables.

In summary, we applied the following steps to design our controller strategies:

1. To design an LQR controller, (24) is linearized around an equilibrium point using the Jacobian linearization framework.
2. Verify the pair of (A, B) is pointwise stabilizable (controllable) at $\tilde{x} = 0$.
3. Find a gain matrix K such that all of the eigenvalues of the closed-loop system are located at the left-half plane, using the pole assignment.

Calculate the state feedback controller (38) gain matrix (K).

Motivated by the LQR problem, SDRE theory was developed to solve the regulation problem for systems with non-linear dynamics. The SDRE technique is an extended linearization control or state-dependent coefficient (SDC) method that provides procedures similar to the LQR to the non-linear regulation problems for both input-non-affine [30] and affine systems with a cost function like (37) [29].

5 | NON-LINEAR STATE FEEDBACK CONTROLLER BASED ON SDRE

In our DC MG model, since the state variables are multiplied by input variables, the system becomes non-linear. Moreover, the exponential term in (17) belongs to the diode in the PV model also adds more non-linearity. Due to the existence of control input u^2 in (20), the system becomes non-affine. In summary, since the whole system is a non-linear-non-affine, we are motivated to develop a control strategy that is capable to regulate the system with the non-linear-non-affine structure. Although a lot of works have been done in this regard, however, this controller has not been examined for DC MG, especially with high non-linear and non-affine structures. Consider the following non-linear-non-affine dynamic system:

$$\dot{x}(t) = f(x) + g(x, u) \tag{40}$$

where $x \in \mathbb{R}^n$ is the state vector, $u \in \mathbb{R}^m$ is the input vector, and $f(0) = 0$ is the equilibrium point of the system. It should be noted that $\mathbb{R}$ is the set of real numbers; $\mathbb{R}^n$ and $\mathbb{R}^m$ are n- and m-dimensional real Euclidean spaces.

It is assumed that the vector functions $f(x)$ and $g(x, u)$ are continuously smooth and non-linear with respect to their arguments in C^α for $\alpha \geq 1$ and one-time differentiable functions for all x and u in Ω. Moreover, these two vector functions are bounded by $t \rightarrow \infty$, and the derivative of function $g(x, u)$ with respect to u is non-zero ($\frac{\partial g(x, u)}{\partial u} \neq 0, x \in \Omega$). The objective of the controller design is to find a control law u (for $t > 0$) that forces the states/outputs of the system (for $t > 0$) to regulate so that the cost function in (37) is minimized. At the next step, the non-linear-non-affine system in (40) should be expressed as a state-dependent linear system or SDC form as follows:

$$\dot{x} = A(x)x + B(x, u)u \tag{41}$$

where $A(x): \Omega \rightarrow \mathbb{R}^{n \times n}$ and $B(x, u): \Omega \rightarrow \mathbb{R}^{n \times m}$. It should be noted that for a function $f(x)$ with $n > 1$ and $f(0) = 0$, there are infinite ways to express the non-linear system in (40) in the SDC form.

Definition: The SDC representation in (41) is pointwise stabilizable in the bounded open set Ω if the pair of $A(x(t)), B(x, u)$ is stabilizable in the linear model for all $(x, u) \in \Omega$ and $t \geq 0$. To find the suboptimal solution for the cost function (37), there are two steps:

1. First, the Hamiltonian equation is written as $H = \frac{1}{2}(x^T Q x + u^T R u) + \lambda^T (A(x(t)x(t)) + g(x, u))$, and the following conditions are applied:

$$\frac{\partial H}{\partial \lambda} = \dot{x}(t), \ \frac{\partial H}{\partial x} = -\dot{\lambda}, \ \frac{\partial H}{\partial u} = 0 \qquad (42)$$

With a few mathematical manipulations, the control law is obtained in the form of: $u = -R^{-1} B^T(x, u) P(x, u) x$.

1. Computing the following equation would lead a solution for $k(x, u)$ [30].

$$A^T(x) P(x, u) + P(x, u) A(x)$$
$$-P(x, u) B(x, u) R^{-1} B^T(x, u) P(x, u) + Q = 0 \quad (43)$$

In [30], the continuity of $P(x, u)$ is proved for its arguments. To analyse the stability of the non-linear-non-affine system, consider the following theorem.

Theorem: The non-linear-non-affine system in (40) with the quadratic cost function in (37) can be stabilized using the feedback control law if the solution of $P(x, u)$ is positive semidefinite.

Proof: Consider the following Lyapunov function [30]:

$$V = x^T P(x, u) x \qquad (44)$$

By taking the derivative of V with respect to t, one can obtain [30]:

$$\dot{V} = x^T \begin{pmatrix} A^T(x) P(x, u) x + P(x, u) A(x) \\ -P(x, u) B(x, u) R^{-1} B^T(x, u) P(x, u) \\ -P(x, u) B(x, u) R^{-1} B^T(x, u) P(x, u) \end{pmatrix} x \quad (45)$$

To ensure the stability of the system, the value of $\dot{V}$ must be negative. By substituting (43) into (45), the following equation can be created [30].

$$\dot{V} = -x^T \left(P(x, u) B(x, u) R^{-1} B^T(x, u) P(x, u) + Q \right) x \qquad (46)$$

In (46), Q is positive semidefinite, R is positive definite, and $P(x, u)$ is positive definite. It can be concluded that the term $B^T(x, u) B(x, u)$ is positive. Therefore, the stability of the system is proven. It should be emphasized that the online control update formulation is used for a system with non-linear-non-affine dynamics. Accordingly, the following equations can be solved repeatedly. Therefore, the updated optimal gain can be
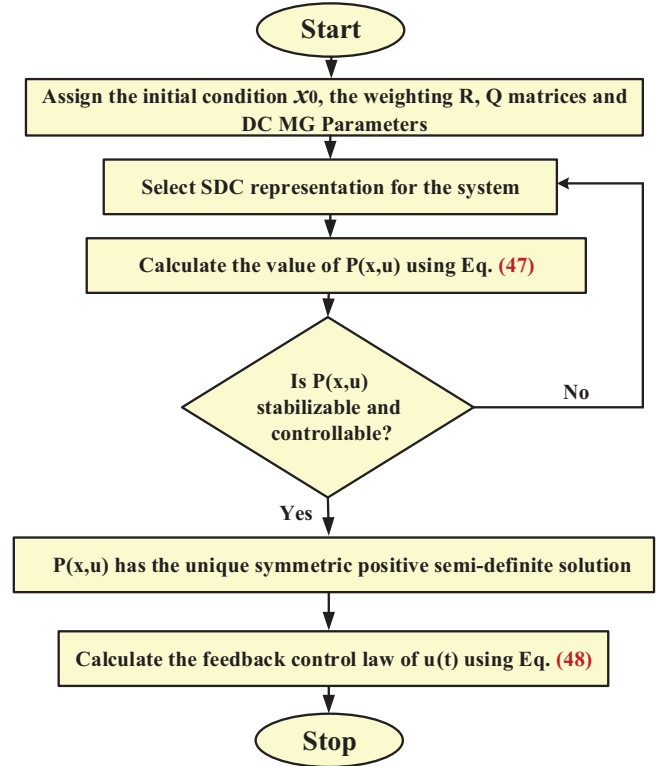

FIGURE 11 Overall flowchart of the studied nonlinear controller using SDRE technique

obtained at each step [30].

$$P^{n+1}(x, u) A^T(x^n) + A^T(x^n) P^{n+1}(x, u)$$
$$-P^{n+1}(x, u) B(x, u) R^{-1} B^T(x^n, u^n) P^{n+1}(x, u) + Q = 0$$
$$\qquad (47)$$

The feedback control law is:

$$u = -R^{-1} B^T(x^n, u^n) P^{n+1}(x, u) x^n \qquad (48)$$

The overall flowchart of the proposed SDRE controller is illustrated in Figure 11. The SDC representation of the non-linear-non-affine DC MG system described in (24) is presented in Appendix B. In this context, it is necessary to ensure that the pair of $(A(x), B(x,u))$ is exactly equal to the non-linear system when multiplied by x and u $(\dot{x}(t) = f(x) + g(x, u))$ [29]. According to the aforementioned conditions, the origin $x = 0 \in \Omega$ is an equilibrium point of the system with $u = 0$, such that $f(0) = 0$ and $B(x, u) \neq 0 \ \forall \ x \in \Omega$ which means that we should move the equilibrium points of the system to the origin. Therefore the equilibrium points have translated $\tilde{x} = x - x^*$. This process is accomplished in Appendix B. In summary, the block diagram of the proposed SDRE controller is shown in Figure 12.

TABLE 3 Specifications of the proposed DC MG

Parameters	Value
Inductors (L_1, L_2, L_3, L_4)	200 (μH)
Capacitors (C_1, C_2, C_3, C_4) (μF)	100, 200, 100, 100
Battery voltage (E)	$E = 120$ V
Battery internal resistance (r)	1 Ω
R_L	5 Ω
R_1, R_2	$R_1 = 144\ \Omega$, $R_2 = 9\ \Omega$
P_{mpp}	1200 W
I_{wind}	10 A
Desired trajectories	$\overset{*}{x}_2 = V_{mpp}$, $\overset{*}{x}_4 = 270$ V, $\overset{*}{x}_6 = 100$ V, $\overset{*}{x}_8 = 200$ V
R and Q	$Q = 10\mathrm{I}_8$, $R = \mathrm{diag}(10, 10, 1, 0.1)$
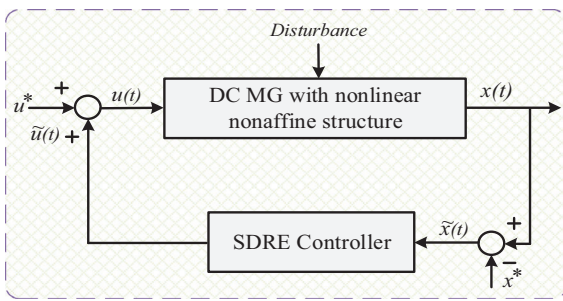
FIGURE 12 Block diagram of the SDRE controller

6 | IMPLEMENTATION RESULTS AND ANALYSIS

In this section, to verify the previous theory, the studied DC MG system shown in Figure 2 is implemented to simulate and analyse the developed controllers in the MATLAB environment. It is assumed that the 1-kW PV source is connected to the main DC bus via a DC/DC boost converter and injects its maximum power. Also, the wind turbine operates at the maximum point and delivers maximum power to the DC MG.

Remark: There are two different assumptions in this paper: The solar irradiance will be change while the load is constant and vice versa; In addition, the wind velocity change while solar irradiance and load are constant. On the other hand, the injected current by the wind turbine (I_{wind}) would change.

Therefore, step load change and illumination changes in terms of irradiance and wind velocity are considered external disturbances. The parameters to conduct the simulation studies are taken from Table 3. The performance of two studied controllers under step load change and illumination change will be evaluated.

6.1 | Load change

A code is written in MATLAB to compute the control law (44). The simulation time is set at 0.06 s, and the time step

is selected as 10^{-6} s. In both simulation simulations, the initial condition and weighting matrices are selected as $x(0) = [1 -1\ 0.2\ 1 -1\ 0.2\ 1 -1]^{\mathrm{T}}$. The performance of the state variables in presence of SDRE and LQR controller is shown in Figure 13. In this case, at $t = 0$ s, the DC MG is operating at the steady state which means the PV delivers maximum power output, the battery is charging, and the wind turbine injects its maximum power as well; however, at $t = 0.02$ s, suddenly, the bus load increases (R_1 decreases from 144 to 100Ω); at $t = 0.04$ s, the DC load decreases (R_2 increases from 9 to 14Ω). When the bus load increases at $t = 0.02$ s, subsequently, the battery will be discharged to compensate power shortage. However, with decreasing DC load at $t = 0.04$ s, the corresponding duty cycle u_3, which is depicted in Figure 14, is adjusted such that to maintain the DC load voltage and then, the battery will be charged again. As can be seen, visually, those dynamic performances which are obtained by applying

SDRE regulator have better than LQR. However, the following findings are expressive:

1. Unfortunately, during load change, it is discovered that some states are not controllable when the LQR controller is applied while the oscillation can be seen in Figure 17 for the case of wind current; thus LQR is not implementable.
2. We consider the following saturation function on the control inputs u_1, u_2, u_3, and u_4 to limit their values to the range of [0,1] [29].

$$Sat\ (u\ (t)\ , u_{\max}) = \begin{cases} u_{\max} & |u\ (t)| > u_{\max} \\ u\ (t) & |u\ (t)| \leq u_{\max} \\ -u_{\max} & |u\ (t)| < -u_{\max} \end{cases} \quad (49)$$

6.2 | Illumination change

In this simulation, the solar irradiance and wind velocity will change according to the following. At $t = 0$ s, the DC MG is operating at steady state which means the PV delivers maximum
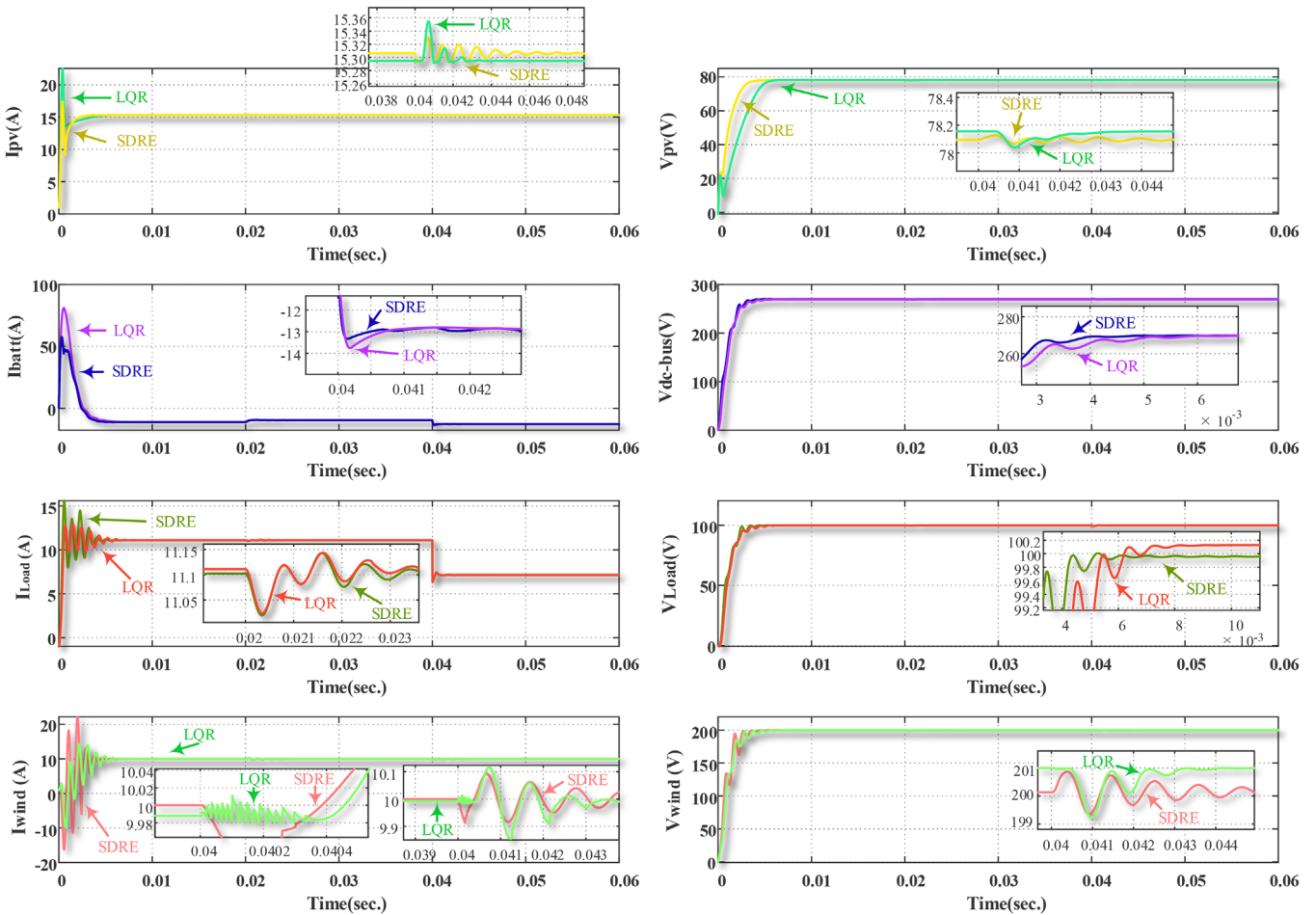
FIGURE 13   Dynamic performance of state variables using LQR and SDRE regulators converge to their desired values under load change

power output, the battery absorbs power, and the wind turbine injects its maximum power as well.

Hence, the PV generates the current $I_{ph} = 16.26$ A, the corresponding output voltage which is obtained by (36) would be computed as $V_{mpp} = 78.15$ V and maximum power of PV therefore is $P_{mpp} = 1196$ W. Moreover, the wind turbine generates its maximum current which is $I_{wind} = 10$ A, the output voltage of the rectifier is set at 200 V, and therefore, wind generates $P_{wind} = 2000$ W. At $t = 0.02$ s, I_{ph} drops to 10 A and the corresponding maximum voltage will be 75.94 V. Subsequently, the PV output power decrease to 712.5 W. Another disturbance occurs at $t = 0.04$ s when I_{ph} decrease from 10 to 5 A and the maximum voltage is 72.79 V. In this case, the resulting output power is 339.69 W. Eventually, at $t = 0.06$ s, the maximum current injected by wind decreases to $I_{wind} = 5$ A. To construct a baseline for comparison, constant state feedback or linear state feedback design is also taken into account and locally are implemented. The simulation results considering two controllers are given in Figures 15 and 16. Accordingly, the battery in DC MG is responsible for power balancing when the first illumination occurs. As can be seen, the battery is charging at $t = 0$ s, however, at $t = 0.02$ s discharges to meet power balance. Moreover, u_3 would be constant during the simulation because the DC

bus voltage is constant and also u_4 is constant till wind velocity remains unchanged. As seen, the dynamic response of constant feedback is suffering from poor performance. At $t = 0.04$ s, the PV output power goes down (5 A), and at the same time wind output power drop to 1000 W. In this case, the battery is being discharged to maintain DC bus voltage. By comparison, it can be said that, by applying the SDRE controller, the oscillation is dramatically decreased while state variables converge to their desired values in a short period of time and settle quickly.

6.3 | A comparison between the proposed method and passivity-based design method

As a comparison between the studied controller and proposed controllers in [24] and [25] the following findings are expressive:

1. Actually, controllers like SDRE ought to compare with LQR since both methods consider optimality in their design procedure, and therefore, the comparison would be fair. However, the simulated system response using SDRE controller
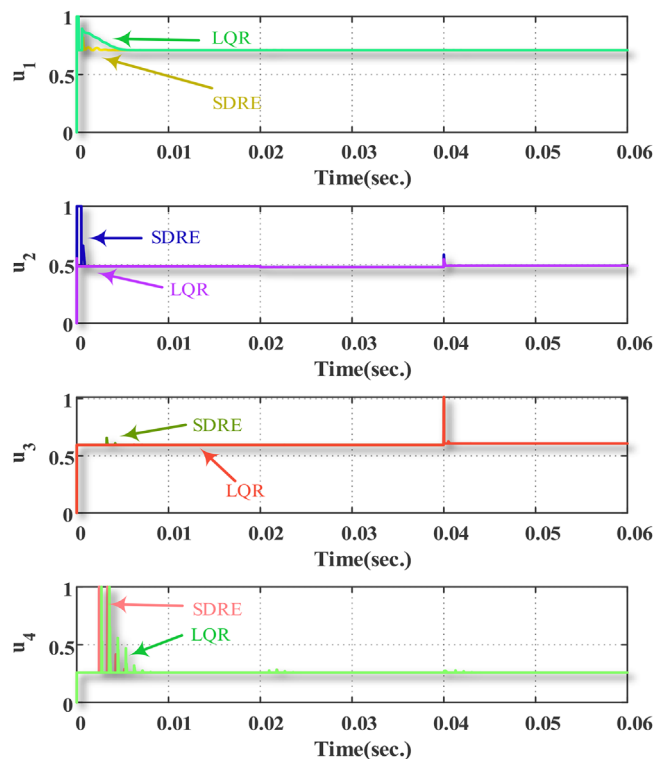
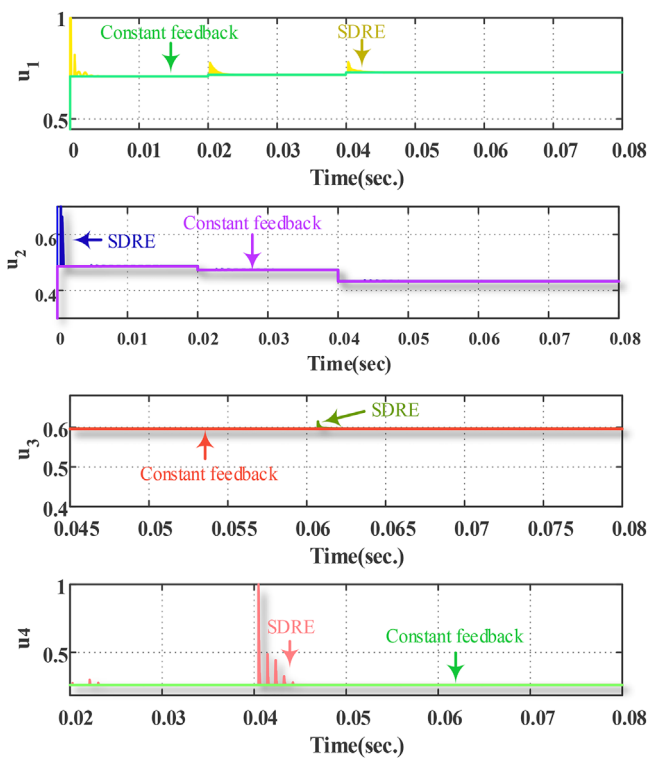**FIGURE 14** A plot of duty cycle waveforms: u_1, u_2, u_3, and u_4

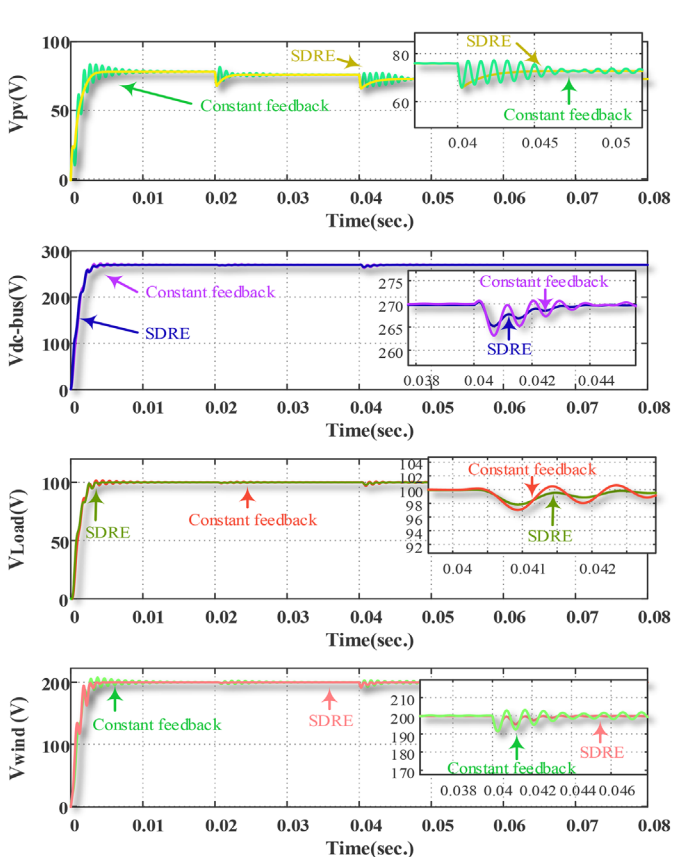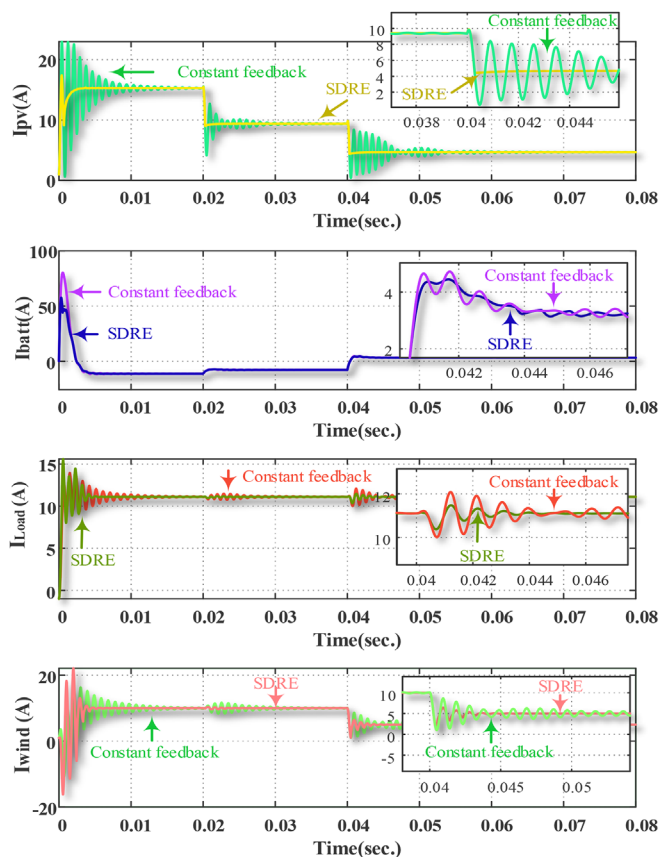**FIGURE 16** A plot of duty cycle waveforms: u_1, u_2, u_3, and u_4

FIGURE 15 Dynamic performance of state variables using SDRE regulators and constant state feedback controller under illumination change
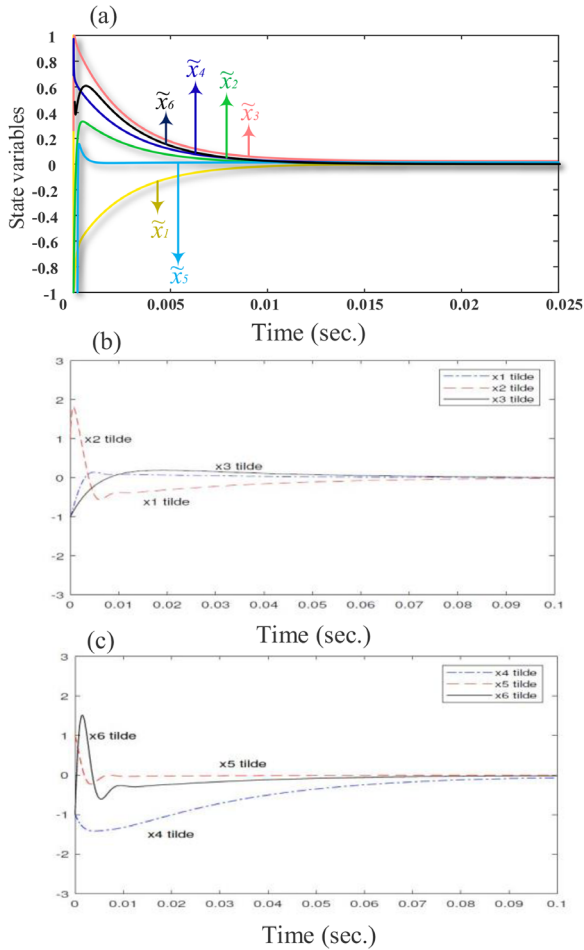
FIGURE 17 Transient response of the SDRE controller (a) Versus passivity-based design method (b) and (c)

with weighting matrices, $Q = 10I_6$, $R = diag(1, 6, 12)$ and passivity-based design method are depicted in Figure 17. In this regard, the performance of the SDRE technique and passivity based design are demonstrated for the case of six non-linear-non-affine system. These figures denote the stability of the closed-loop system and dynamic performance as well.

2. It is assumed that either solar irradiance or other parameters remain unchanged. On the other hand, in both simulations zero would be the nominal values of currents and voltages after translation. Both simulation are performed under the same initial conditions $\tilde{x} = [1 \; -1 \; 0.2 \; 1 \; -1 \; 0.2]^T$ and $\tilde{x}$ (or x tilde) is the deviation from the steady state value. The simulation results are plotted in Figure 17, where it shows that both controllers successfully regulate the system states to their equilibria.

3. One of the difference between the two control schemes is that the proposed SDRE technique here for output regulation is only locally valid which means the system works near its steady-state operating point, while the passivity-based design works globally [25, 29].

4. Another differences between the two methods are the passivity-based design cannot be applied to time-varying

tracking problems but the SDRE approach can effectively use to address time varying tracking problems [25, 29].

7 | CONCLUSIONS

In this study, comprehensive design, mathematical modelling, control, and analysis of a wind/PV/battery based DC MG with multiple DC/DC converters and loads were performed. To this end, first, detailed modelling of the PV source was discussed; then, the obtained model for the PV was connected to the main DC bus by forming a boost converter. Afterward, the non-linear-non-affine state-space model of the DC MG in the form of $\dot{x} = f(x, u)$ was developed. The non-linear-non-affine model of the DC MG has linearized around an equilibrium point. Time-domain simulations for the linear-non-linear models showed that all state variables converged to its equilibrium point, hence proving the validity of the linearized model. Moreover, stability analysis of the linearized system was carried out using an eigenvalue diagram. In this paper, for the first time, the SDRE technique was performed to find a suboptimal solution for a class of DC MG with a non-linear-non-affine dynamic model. The numerical results showed that the proposed method successfully regulated the output variables. Furthermore, the effectiveness of the designed SDRE controller was compared with the classic LQR and linear state feedback controller. Eventually, the performance of the SDRE regulator has been evaluated under illumination and load change shows that the transient performance is dramatically improved.

CONFLICT OF INTEREST
Authors do not have any conflict of interest.

DATA AVAILABILITY STATEMENT
Research data are not shared.

ORCID
Hossein Torkaman https://orcid.org/0000-0002-6342-0972
Mehdi Bagheri https://orcid.org/0000-0002-8078-9173

REFERENCES
1. Ghadiriyan, S., Rahimi, M.: Mathematical representation, stability analysis and performance improvement of DC microgrid system comprising hybrid wind/battery sources and CPLS. IET Gener. Transm. Distrib. 13(10), 1845–1855 (2019)
2. Torkaman, H., Afjei, E., Keyhani, A., Poursmaeil, M.: Control and management of a hybrid AC/DC microgrid based on Γ-Z-source interlinking converter and multi-port converter. IET Gener. Transm. Distrib. 14(14), 2847–2856 (2020)
3. Abhishek, A., Ranjan, A., Devassy, S., Verma, B.K., Ram, S.K. Dhakar, A.K.: Review of hierarchical control strategies for DC microgrid. IET Renew. Power Gener. 14(10), 1631–1640 (2020)
4. Torkaman, H., Khosrogorji, S., Keyhani, A.: Multi-input converters for distributed energy resources in microgrids. Microgrids for Rural Areas: Research and Case Studies, pp. 279–330, IET, London (2020)

5. Melath, G., Rangarajan, S., Agarwal, V.: Comprehensive power management scheme for the intelligent operation of photovoltaic-battery based hybrid microgrid system. IET Renew. Power Gener. 14(10), 1688–1698 (2020)

6. Golkhandan, R.K., Torkaman, H., Aghaebrahimi, M.R., Keyhani, A., Load frequency control of smart isolated power grids with high wind farm penetrations. IET Renewable Power Gener. 14(7), 1228–1238 (2020)

7. Einan, M., Torkaman, H., Pourgholi, M.: Optimized fuzzy-cuckoo controller for active power control of battery energy storage system, photovoltaic, fuel cell and wind turbine in an isolated micro-grid. Batteries 3(23), 1–18 (2017)

8. Batzelis, E.I., Papathanassiou, S.A.: A method for the analytical extraction of the single-diode PV model parameters. IEEE Trans. Sustainable Energy 7(2), 504–512 (2016)

9. Silva, E.A., Bradaschia, F., Cavalcanti, M.C., Nascimento, A.J., Michels, L., Pietta, L.P.: An eight-parameter adaptive model for the single diode equivalent circuit based on the photovoltaic module's physics. IEEE J. Photovoltaics 7(4), 1115–1123 (2017)

10. Arabshahi, M.R., Torkaman, H., Keyhani, A.: A method for hybrid extraction of single-diode model parameters of photovoltaics. Renewable Energy 158, 236–252 (2020)

11. Manoharan, P., Subramaniam, U., Babu, T.S., Padmanaban, S., Holm-Nielsen, J.B., Mitolo, M., Ravichandran, S.: Improved perturb & observation maximum power point tracking technique for solar photovoltaic power generation systems. IEEE Syst. J. 15, 3024–3035 (2020)

12. Rezk, H., Aly, M., Al-Dhaifallah, M., Shoyama, M.: Design and hardware implementation of new adaptive fuzzy logic-based MPPT control method for photovoltaic applications. IEEE Access 7, 106427–106438 (2019)

13. Solórzano, J., Egido, M.: Automatic fault diagnosis in PV systems with distributed MPPT. Energy Convers. Manage. 76, 925–934 (2013)

14. Kumar, P., Jain, G., Palwalia, D.K.: Genetic algorithm based maximum power tracking in solar power generation. In: International Conference on Power and Advanced Control Engineering, Bengaluru, India, pp. 1–6 (2015)

15. Lenz, E., Pagano, D.J.: Nonlinear Control for bidirectional power converter in a DC microgrid. IFAC Proc. 46(23), 359–364 (2013)

16. Stramosk, V., Pagano, D.J.: Nonlinear control of a bidirectional DC-DC converter operating with boost-type constant-power loads. In: Brazilian Power Electronics Conference, Gramado, Brazil, pp. 305–310 (2013)

17. Peyghami, S., Mokhtari, H., Blaabjerg, F.: Autonomous power management in LvDC microgrids based on a superimposed frequency droop. IEEE Trans. Power Electron. 33(6), 5341–5350 (2017)

18. Jiang, W., Yang, C., Liu, Z., Liang, M., Li, P., Zhou, G.: A hierarchical control structure for distributed energy storage system in DC micro-grid. IEEE Access 7, 128787–128795 (2019)

19. Sanchez, S., Soloot, A.H., Molinas, M.: Stability influence of renewable energy systems: connection to DC nanogrids. In: IEEE 17th Workshop on Control and Modeling for Power Electronics, Trondheim, Norway, pp. 1–8 (2016)

20. Liu, J., Zhang, W., Rizzoni, G.: Robust stability analysis of DC microgrids with constant power loads. IEEE Trans. Power Syst. 33(1), 851–860 (2017)

21. Haroun, R., El Aroudi, A., Cid-Pastor, A., Vidal-Idiarte, E., Valderrama-Blavi, H., Martinez-Salamero, L.: Modelling and control of modular DC-nanogrids based on loss-free resistors. IEEE Access 8, 33305–33317 (2020)

22. Roy, T.K., Mahmud, M.A., Oo, A.M.T., Haque, M.E., Muttaqi, K.M., Mendis, N.: Nonlinear adaptive backstepping controller design for islanded DC microgrids. IEEE Trans. Ind. Appl. 54(3), 2857–2873 (2018)

23. Singh, S., Fulwani, D., Kumar, V.: Robust sliding-mode control of DC/DC boost converter feeding a constant power load. IET Power Electron. 8(7), 1230-1237 (2015)

24. Lin, W., Rattanamongkhonkun, K., Pongvuthithum, R.: L_Gv-Type Adaptive Controllers for Uncertain Non-Affine Systems and Application to a Dc-Microgrid with Pv and Battery. IEEE Trans. Autom. Control 64(5), 2182-2189 (2018)

25. Sun, J., Lin, W., Hong, M., Loparo, K.A.: Voltage Regulation of Dc-Microgrid with Pv and Battery: A Passivity Method. IFAC-PapersOnLine 52(16), 753–758 (2019)

26. Habib, M., Khoucha, F., Harrag, A.: Ga-based robust LQR controller for interleaved boost DC–DC converter improving fuel cell voltage regulation. Electr. Power Syst. Res. 152, 438–456 (2017)

27. Wang, L., Ni, H., Zhou, W., Pardalos, P.M., Fang, J., Fei, M.: MBPOA-based LQR controller and its application to the double-parallel inverted pendulum system. Eng. Appl. Artif. Intell. 36, 262–268 (2014)

28. Liu, C., Pan, J., Chang, Y.: PID and LQR trajectory tracking control for an unmanned quadrotor helicopter: Experimental studies. In: 35th Chinese Control Conference, Chengdu, China, pp. 10845–10850 (2016)

29. Çimen, T.: Systematic and effective design of nonlinear feedback controllers via the state-dependent Riccati equation (SDRE) method. Ann. Rev. Control 34(1), 32–51 (2010)

30. Nekoo, S.R., Geranmehr, B.: Nonlinear observer-based optimal control using the state-dependent Riccati equation for a class of non-affine control systems. J. Control Eng. Appl. Inf. 16(2), 5–13 (2014)

31. Abdali, A., Mazlumi, K., Guerrero, J.M.: Integrated control and protection architecture for islanded PV-battery DC microgrids: Design, analysis and experimental verification. Appl. Sci. 10(24), 8847 (2020)

32. Chatterjee, A., Keyhani, A., Kapoor, D.: Identification of photovoltaic source models. IEEE Trans. Energy Convers. 26(3), 883–889 (2011)

33. Orioli, A., Di Gangi, A.: A procedure to calculate the five-parameter model of crystalline silicon photovoltaic modules on the basis of the tabular performance data. Appl. Energy 102, 1160–1177 (2013)

34. UD-185MF5 photovoltaic module: https://www.mitsubishielectricsolar.com/images/uploads/documents/specs/UD5_spec_sheet_185W.pdf (2021). Accessed May 2021

35. Hejri, M., Mokhtari, H., Azizian, M.R., Ghandhari, M., Söder, L.: On the parameter extraction of a five-parameter double-diode model of photovoltaic cells and modules. IEEE J. Photovoltaics 4(3), 915–923 (2014)

36. Chen, J., Lin, T., Wen, C., Song, Y.: Design of a unified power controller for variable-speed fixed-pitch wind energy conversion system. IEEE Trans. Indust. Electron. 63(8), 4899–4908 (2016)

37. Erickson, R.W., Maksimovic, D., Fundamentals of Power Electronics, Springer Science & Business Media, Berlin (2007))

38. Kumar, E.V., Jerome, J., Raaja, G.: State dependent Riccati equation based nonlinear controller design for ball and beam system. Proc. Eng. 97, 1896–1905 (2014)

39. Taylor Expansion: Available At: https://www.sciencedirect.com/topics/engineering/taylor-expansion (2021). Accessed May 2021

APPENDIX A

It is noteworthy that the symbol of the equilibrium point variables is specified by " * ". Suppose that $\overset{*}{x}$ and $\overset{*}{u}$ are the equilibrium points; then, the actual state and input variables can be written as: $x = \overset{*}{x} + \delta x$ and $u = \overset{*}{u} + \delta u$. The "$\delta$" denotes the small variation around the equilibrium point. Substituting the values of x and u, we obtain:

$$\dot{\delta} x = f\left(\overset{*}{x} + \delta x, \overset{*}{u} + \delta u\right) \tag{A.1}$$

Now, using Taylor series expansion and neglecting the higher-order terms (higher than 1st) gives [39]:

$$\dot{\delta}x \approx f\left(\overset{*}{x}, \overset{*}{u}\right) + \frac{\partial f}{\partial x}\Big|_{\substack{x = \overset{*}{x} \\ u = \overset{*}{u}}} \delta x + \frac{\partial f}{\partial x}\Big|_{\substack{x = \overset{*}{x} \\ u = \overset{*}{u}}} \delta u \qquad \text{(A.2)}$$

However, $f(\overset{*}{x}, \overset{*}{u}) = 0$; therefore: $\dot{\delta}x \approx \frac{\partial f}{\partial x}\Big|_{\substack{x = \overset{*}{x} \\ u = \overset{*}{u}}} \delta x +$

$\frac{\partial f}{\partial x}\Big|_{\substack{x = \overset{*}{x} \\ u = \overset{*}{u}}} \delta u$. The constant matrices are defined as follows:

$$A = \frac{\partial f}{\partial x}\Big|_{\substack{x = \overset{*}{x} \\ u = \overset{*}{u}}}, \quad B = \frac{\partial f}{\partial x}\Big|_{\substack{x = \overset{*}{x} \\ u = \overset{*}{u}}} \qquad \text{(A.3)}$$

With matrices A and B, the linearized state-space equations of the system are given below:

$$\dot{\delta}x \approx A\,\delta x + B\,\delta u \qquad \text{(A.4)}$$

APPENDIX B

Prior to controller design using the SDRE, translation is needed. Translation means moving the equilibrium points to the origin $\tilde{x} = x - \overset{*}{x}$ and $\tilde{u} = u - \overset{*}{u}$. Hence, after the translation, to implement the proposed SDRE controller, an SDC representation is needed. As discussed in Section 5, there are infinite ways to form the state-dependent matrices. However, our SDC representation is given below:

$$\tilde{A}(x) =$$

$$\begin{bmatrix}
0 & \frac{1}{L_1} & 0 & a_{14} & 0 & 0 & 0 & 0 \\
-\frac{1}{C_1} & a_{22} & 0 & 0 & 0 & 0 & 0 & 0 \\
0 & 0 & -\frac{r}{L_2} & -\frac{\overset{*}{u_2}}{L_2} & 0 & 0 & 0 & 0 \\
a_{41} & 0 & \frac{\overset{*}{u_2}}{C_2} & \frac{-1}{R_1 C_2} & a_{45} & 0 & a_{47} & 0 \\
0 & 0 & 0 & a_{54} & a_{55} & -\frac{1}{L_3} & 0 & 0 \\
0 & 0 & 0 & 0 & \frac{1}{C_3} & \frac{-1}{R_2 C_3} & 0 & 0 \\
0 & 0 & 0 & a_{74} & 0 & 0 & 0 & \frac{1}{L_4} \\
0 & 0 & 0 & 0 & 0 & 0 & -\frac{1}{C_4} & 0
\end{bmatrix}$$

$$\text{(B.1)}$$

where:

$$a_{14} = -\frac{(1 - \overset{*}{u_1})}{L_2}$$

$$a_{22} = -\frac{1}{C_1}\left(\frac{1}{R_{sh}} + \frac{I_o}{\tilde{x}_2} e^{a(\tilde{x}_1 R_s + \overset{*}{x}_2)}\left(e^{a(\tilde{x}_1 R_s + \tilde{x}_2)} - 1\right)\right)$$

$$a_{41} = \frac{(1 - \overset{*}{u_1})}{C_2} \quad a_{45} = \frac{-(1 - \overset{*}{u_3})}{C_2} \quad a_{47} = \frac{(1 - \overset{*}{u_4})}{C_2}$$

$$a_{54} = \frac{(1 - \overset{*}{u_3})}{L_3} \quad a_{55} = \frac{R_L(1 + \overset{*}{u_3})^2}{L_3}$$

$$a_{74} = \frac{(1 - \overset{*}{u_4})}{L_2}$$

$$\tilde{B}(x, u) =$$

$$\begin{bmatrix}
\frac{1}{L_1}\left(\overset{*}{x_4} + \tilde{x}_4\right) & 0 & 0 & 0 \\
0 & 0 & 0 & 0 \\
0 & \frac{-r}{L_2}\left(\overset{*}{x_4} + \tilde{x}_4\right) & 0 & 0 \\
\frac{1}{C_2}\left(\overset{*}{x_1} + \tilde{x}_1\right) & \frac{1}{C_2}\left(\overset{*}{x_3} + \tilde{x}_3\right) & \frac{1}{C_2}\left(\overset{*}{x_5} + \tilde{x}_5\right) & \frac{1}{C_2}\left(\overset{*}{x_7} + \tilde{x}_7\right) \\
0 & 0 & b_{53} & 0 \\
0 & 0 & 0 & 0 \\
0 & 0 & 0 & \frac{1}{L_4}\left(\overset{*}{x_4} + \tilde{x}_4\right) \\
0 & 0 & 0 & 0
\end{bmatrix}$$

$$\text{(B.2)}$$

where:

$$b_{53} = \frac{1}{L_3}\left(2R_L(\overset{*}{x_5} + \tilde{x}_5) - (\overset{*}{x_4} + \tilde{x}_4) - R_L(\overset{*}{x_5} + \tilde{x}_5)\tilde{u}_3\right).$$